AGU PUBLICATIONS

Geophysical Research Letters

RESEARCH LETTER
10.1002/2017GL076509

Key Points:
- For the first time, fast electron jet is observed at dipolarization front
- This jet is responsible for current and energy conversion at dipolarization front
- Quantitatively, the partition of energy conversion is $\mathbf{E} \cdot \mathbf{j}_e \approx 2\,\mathbf{E} \cdot \mathbf{j}_i$

Correspondence to:
H. S. Fu,
huishanf@gmail.com

Citation:
Liu, C. M., Fu, H. S., Vaivads, A., Khotyaintsev, Y. V., Gershman, D. J., Hwang, K.-J., … Le Contel, O. (2018). Electron jet detected by MMS at dipolarization front. *Geophysical Research Letters*, *45*, 556–564. https://doi.org/10.1002/2017GL076509

Received 23 NOV 2017
Accepted 3 JAN 2018
Accepted article online 8 JAN 2018
Published online 24 JAN 2018

Electron Jet Detected by MMS at Dipolarization Front

C. M. Liu[1], H. S. Fu[1], A. Vaivads[2], Y. V. Khotyaintsev[2], D. J. Gershman[3], K.-J. Hwang[4], Z. Z. Chen[1], D. Cao[1], Y. Xu[1], J. Yang[1], F. Z. Peng[1], S. Y. Huang[5], J. L. Burch[4], B. L. Giles[3], R. E. Ergun[6], C. T. Russell[7], P.-A. Lindqvist[8], and O. Le Contel[9]

[1]School of Space and Environment, Beihang University, Beijing, China, [2]Swedish Institute of Space Physics, Uppsala, Sweden, [3]NASA Goddard Space Flight Center, Greenbelt, MD, USA, [4]Southwest Research Institute, San Antonio, TX, USA, [5]School of Electronic and Information, Wuhan University, Wuhan, China, [6]Laboratory of Atmospheric and Space Physics, University of Colorado Boulder, Boulder, CO, USA, [7]Department of Earth and Space Sciences, University of California, Los Angeles, CA, USA, [8]KTH Royal Institute of Technology, Stockholm, Sweden, [9]LPP, CNRS, Palaiseau, France

Abstract Using MMS high-resolution measurements, we present the first observation of fast electron jet (V_e ~2,000 km/s) at a dipolarization front (DF) in the magnetotail plasma sheet. This jet, with scale comparable to the DF thickness (~ 0.9 d_i), is primarily in the tangential plane to the DF current sheet and mainly undergoes the $\mathbf{E} \times \mathbf{B}$ drift motion; it contributes significantly to the current system at the DF, including a localized ring-current that can modify the DF topology. Associated with this fast jet, we observed a persistent normal electric field, strong lower hybrid drift waves, and strong energy conversion at the DF. Such strong energy conversion is primarily attributed to the electron-jet-driven current ($\mathbf{E} \cdot \mathbf{j}_e \approx 2\,\mathbf{E} \cdot \mathbf{j}_i$), rather than the ion current suggested in previous studies.

1. Introduction

Dipolarization fronts (DFs), characterized by the abrupt increase of magnetic field B_z (e.g., Fu et al., 2012a; Nakamura et al., 2002; Runov et al., 2009; Schmid et al., 2016; Sergeev et al., 2009) and usually preceded by a small B_z dip structure (e.g., Huang et al., 2012; Yao et al., 2015), are frequently observed as earthward-propagating tangential discontinuities (e.g., Fu et al., 2012b; Khotyaintsev et al., 2011; Lu et al., 2013) in bursty bulk flows (BBFs) (e.g., Angelopoulos et al., 1992; Cao et al., 2006, 2008; Ma et al., 2009) in the Earth's magnetotail. They play a significant role in flux transport and energy conversion during substorms (e.g., Angelopoulos et al., 2013; Huang, Fu, et al., 2015; Hwang et al., 2011; Liu et al., 2013) and have been suggested as consequences of unsteady magnetic reconnection in both simulations (e.g., Sitnov et al., 2009) and observations (e.g., Fu, Cao, et al., 2013).

DFs can propagate coherently toward the Earth over a long distance after their formation near the reconnection site in the midtail (e.g., Runov et al., 2009). During earthward propagation of DFs, strong wave activity, such as lower hybrid drift waves (e.g., Divin, Khotyaintsev, Vaivads, & André, 2015; Khotyaintsev et al., 2011; Zhou et al., 2009), large-amplitude magnetosonic waves (Huang, Yuan, et al., 2015; Zhou et al., 2014), and broadband electrostatic waves (Yang et al., 2017), has been observed at the DF. The DF has also been suggested as important energy conversion site (e.g., Angelopoulos et al., 2013; Huang, Fu, et al., 2015; Khotyaintsev et al., 2017) due to intense currents and electric fields at the front. Flux pileup regions (FPRs) (e.g., Fu et al., 2011; Khotyaintsev et al., 2011) or dipolarizing flux bundles (e.g., Liu et al., 2013) behind DFs have been suggested to be favorable places for suprathermal electron acceleration (e.g., Ashour-Abdalla et al., 2011; Birn et al., 2013; Duan et al., 2014; Fu et al., 2011; Fu, Khotyaintsev, et al., 2013; Gabrielse et al., 2012; Liu, Fu, Xu, Wang, et al., 2017; Lu et al., 2016; Pan et al., 2012; Wu et al., 2013), wave-particle interactions (e.g., Breuillard et al., 2016; Fu et al., 2014; Huang et al., 2012; Hwang et al., 2014; Khotyaintsev et al., 2011; Panov et al., 2013), and pitch angle evolution (e.g., Fu, Khotyaintsev, Vaivads, André, Sergeev, et al., 2012; Liu, Fu, Xu, Cao, & Liu, 2017; Liu, Fu, Cao, et al., 2017).

So far, particle and wave dynamics in the vicinity of DFs, particularly inside the FPRs, have been well investigated. However, plasma dynamics right at the front remains an open issue hitherto, owing to the scarcity of high-resolution multipoint measurements at the front. Comparing to previous spacecraft missions (e.g., Cluster and Time History of Events and Macroscale Interactions during Substorms (THEMIS)), the recently launched Magnetospheric Multiscale (MMS) mission (Burch et al., 2015) provides highly improved particle measurements at unprecedented temporal resolution and has small separations, enabling

detailed investigation of particle dynamics and wave characteristics at the front. Using MMS measurements, the global distribution of DFs (Schmid et al., 2016), whistler waves behind DFs (Breuillard et al., 2016), and current structures at DFs (Yao et al., 2017) have recently been investigated. However, in these studies, the DFs were detected in the commissioning phase of MMS, when the particle measurements were unavailable or not well calibrated, and consequently, the particle dynamics at DFs was not discussed there.

Recently, MMS has proceeded to its first tail season (after May 2017) with high-resolution measurements of particles, providing an opportunity to address this issue. In this study, we use the MMS measurements in its first tail season to study the particle dynamics at the DF. We particularly focus on the characteristics of electron flow at the front, which could not be directly measured by previous spacecraft (e.g., Cluster and THEMIS). For the first time, we reveal the partition of energy conversion at the DF, which is crucial but could not be resolved by previous spacecraft as well.

2. Observations

An event of interest was observed by MMS on 28 May 2017, when the four MMS spacecraft were located at [−19.6, −12.6, 2.1] Earth radii in geocentric solar magnetospheric (GSM) coordinates, and the MMS constellation was in a tetrahedron formation with ~57 km separation. Note that such a separation (~7 d_e, $d_e = c/\omega_{pe}$ is local electron initial length) is much smaller than that of Cluster (~200 km) and thus allows us to investigate particle dynamics at electron scale. FIELDS EDP (Ergun et al., 2014; Lindqvist et al., 2014), FluxGate magnetometer (Russell et al., 2014), and search-coil magnetometer (Le Contel et al., 2014) data for electric and magnetic fields and Fast Plasma Investigation (FPI; Pollock et al., 2016) data for particles are used in the present study. All the data are shown in GSM coordinates unless noted otherwise.

Figure 1 shows the DF event observed by the four MMS spacecraft from 06:06:00 to 06:07:00 UT. Due to the small separation, four spacecraft provided very similar data. During the whole period, the x component of the magnetic field is small ($|B_x| < 5$ nT; see Figure 1d) and the z component is dominant, indicating that MMS were located in the neutral sheet. The DF was observed at ~06:06:24 UT when B_z increases dramatically from 6 to 16 nT (Figure 1c). The negative spacecraft potential—an indication of the plasma number density (e.g., Hwang et al., 2011)—decreases sharply during the DF crossing (Figure 1f). Using multispacecraft timing analysis, we determine the normal velocity of the DF as 210.7 * [0.68, 0.68, −0.26] km/s (GSM). Considering that the DF crossing lasts ~1.5 s, the DF thickness is about 316 km or equivalently 0.9 d_i, where $d_i = c/\omega_{pi}$ is the local ion inertial length, given the density of 0.3/cm^3.

Figure 2 presents MMS1 observation of the DF crossing from 06:06:20.0 to 06:06:30.0 UT. As can be seen, B_z stays steady at ~7 nT (Figure 2a) in the ambient plasma before 06:06:23.0 UT. The DF, characterized by sharp increase of B_z from 6 nT to 16 nT (Figure 2a), is identified between 06:06:23.5 and 06:06:25.0 UT. Ahead of the DF, a small B_z dip, indicated by the drop of B_z from 7 nT to 6 nT (Figure 2a), is clearly observed from 06:06:23.0 to 06:06:23.5 UT. The FPR behind the DF, characterized by strong B_z (~15 nT, Figure 2a), is encountered after 06:06:25.0 UT. Plasma density is displayed in Figure 2b, in which we see good agreement between the ion and electron density. As can be seen, electron density is ~0.5/cm^3 in the ambient plasma, with little variation inside the B_z dip. Across the DF, such density drops sharply to ~0.3/cm^3 (Figure 2b). This DF features both a sharp B_z increase and a sharp density decease, comparable to the typical values (e.g., Fu et al., 2012a; Runov et al., 2009).

Figures 2c and 2d show the ion and electron velocities. Note that the MMS/FPI ion data may be contaminated by background radiation, which can cause the distortion of the ion moments. In the event, we find good agreement between the electron and ion density (Figure 2b) and no intense background radiation in the ion spectrum (Figure 2h). We also find that the ions are magnetized in the ambient plasma and the flux pileup region behind the DF (see discussion below). Therefore, the ion data in this event should be reliable. As can be seen, the DF was embedded inside a small BBF. Ion velocity roughly stays at 200 km/s in the ambient plasma but clearly decreases (from 220 km/s to 80 km/s; see Figure 2d) at the DF. This localized reduction of ion velocity may indicate that ion jet is impeded by the DF, since the DF moves slower than the BBF. Such ion-front interaction has also been reported by recent simulations (e.g., Drake et al., 2014). Behind the DF, the ion velocity increases back to the background level. Electron velocity is

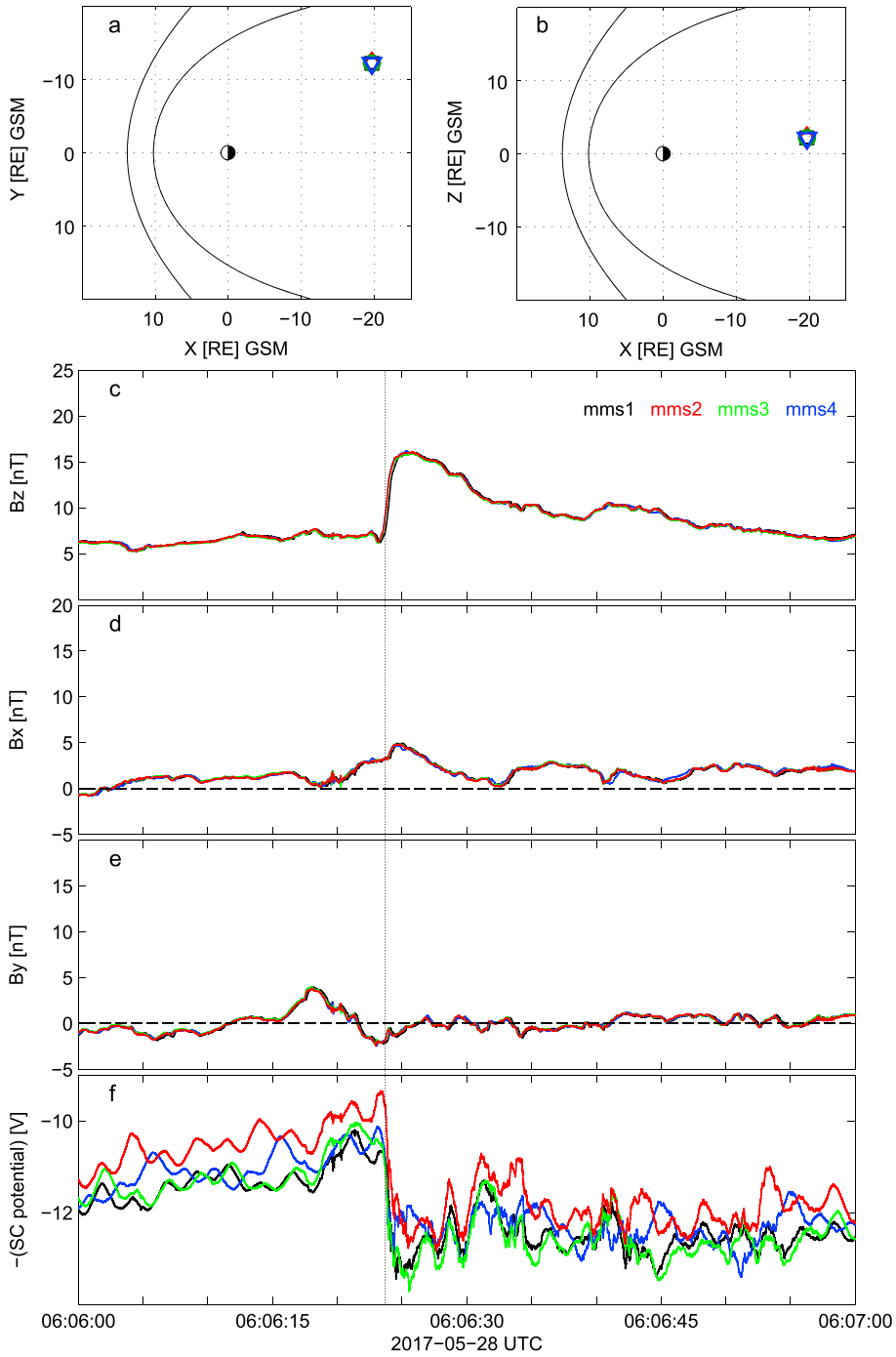

Figure 1. Four MMS spacecraft observations during 28 May 2017, 0606–0607 UT. MMS locations in (a) *X-Z* plane and (b) *X-Y* plane in the GSM coordinates, respectively. The magnetic field components in the (c) z_{GSM}, (d) x_{GSM}, and (e) y_{GSM} directions; (f) the negative spacecraft potential indicative of the electron density. MMS1-MMS4 data are shown in black, red, green, and blue, respectively.

fluctuating during the whole interval but clearly increases across the DF, with V_x, V_y, and V_z up to 1,500 km/s, 1,400 km/s, and 1,000 km/s, respectively (Figure 2c). Electron total velocity reaches up to ~2,000 km/s at ~06:06:24.1 UT (see the dashed line in Figure 2c). Note that the fast electron jet has scale comparable to the DF thickness, consistent with DF current scale suggested by previous studies (e.g., Fu et al., 2012b; Runov et al., 2011).

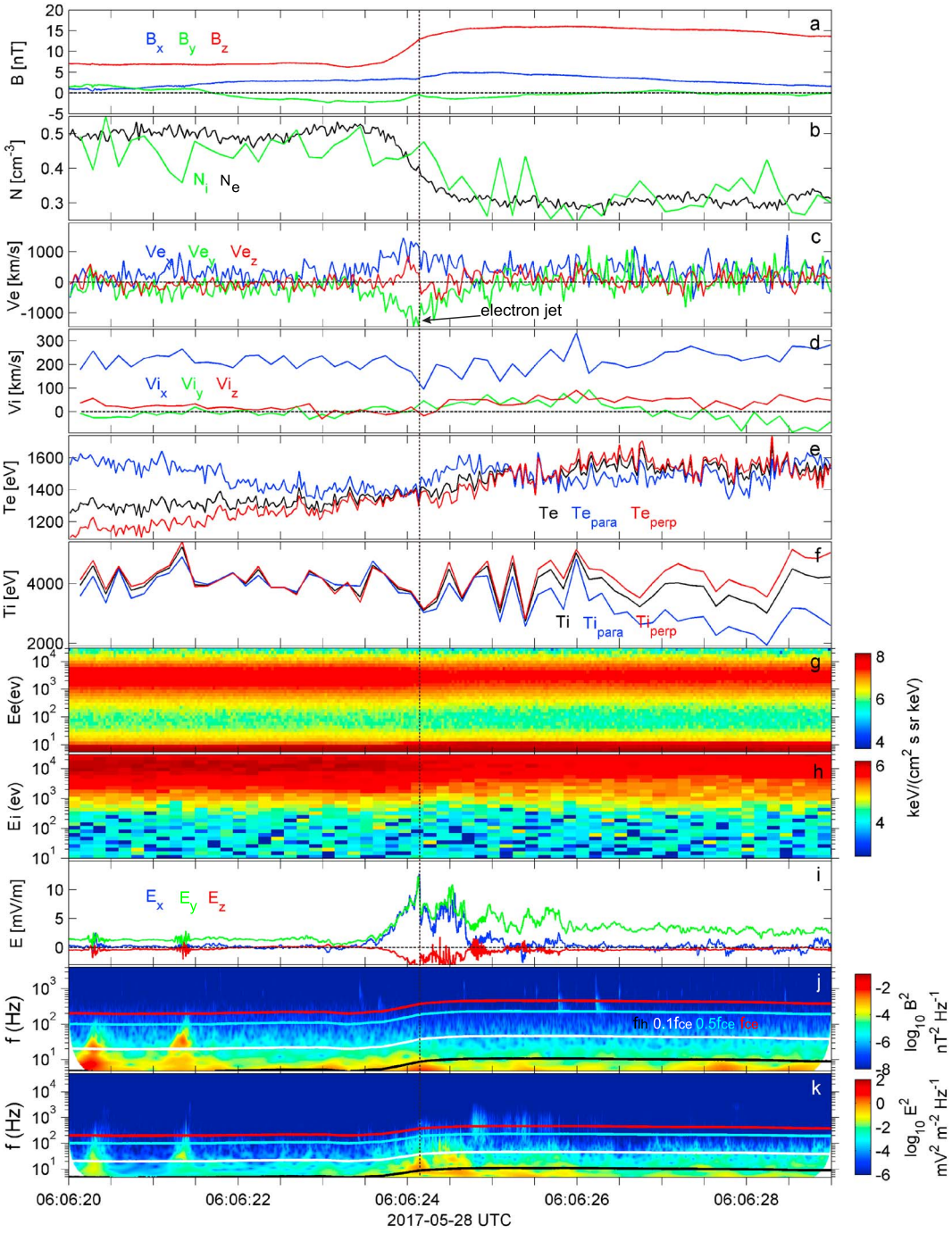

Figure 2. MMS1 observations of DF event from 06:06:20 to 06:06:30 UT. (a) The x_{GSM}, y_{GSM}, and z_{GSM} components of magnetic field; (b) electron and ion density; (c) the x_{GSM}, y_{GSM}, and z_{GSM} components of ion velocity; (d) the x_{GSM}, y_{GSM}, and z_{GSM} components of electron velocity; (e) electron parallel temperature, perpendicular temperature, and total temperature; (f) ion parallel temperature, perpendicular temperature, and total temperature; (g) electron spectrum; (h) ion spectrum; (i) the x_{GSM}, y_{GSM}, and z_{GSM} components of the electric field; (j) the power spectral density for magnetic field; (k) the power spectral density for electric field. The red, cyan, white, and black lines in the bottom two panels represent f_{ce}, 0.5 f_{ce}, 0.1 f_{ce}, and f_{lh}, with f_{ce} and f_{lh} denoting the electron gyrofrequency and the lower hybrid frequency, respectively.

Figures 2e and 2f display the electron and ion temperature. Clearly, electron parallel temperature is larger than perpendicular temperature in the ambient plasma. Such parallel anisotropy gradually abates (parallel temperature decreases, while perpendicular temperature increases) ahead of the DF and changes into isotropy at the jet, possibly due to the adiabatic heating of electrons by contracting magnetic flux tubes (e.g., Fu et al., 2011). Behind the jet peak, electron parallel temperature is enhanced. Such increase of electron parallel temperature is not attributed to the influence of parallel anisotropy inside the ambient plasma since the DF is typically a tangential discontinuity (e.g., Fu et al., 2012b; Khotyaintsev et al., 2011). It also cannot be considered as a consequence of adiabatic effect because the magnetic field strength increases behind the jet (Figure 2a). Inside the FPR, both the electron and ion perpendicular temperatures are slightly higher than their parallel temperature, due to perpendicular heating resulting from the enhanced magnetic field strength. During the whole event, we notice that no sharp change of electron temperature and electron spectrum is observed across the DF, indicating that efficient electron heating/acceleration is absent in the vicinity of the DF.

Figures 2i–2k show the DC electric field and high-frequency waves. In the quiet plasma sheet ahead of DF, electric field is steady (E_x ~−2 mV/m, E_y ~1.5 mV/m, E_z ~0 mV/m; see Figure 2i). Inside the B_z dip, E_y drops to 0.5 mV/m, while E_x and E_z remain constants. Across the DF, electric field increases dramatically, with E_x, E_y, and E_z reaching 10 mV/m, 12 mV/m, and −5 mV/m, respectively (Figure 2i). This localized electric field in the electron jet corresponds to the narrow band waves between f_{lh} and 0.1 f_{ce} (see Figure 2k). Such waves are electrostatic, since no corresponding signatures are observed in the magnetic field spectrum (Figure 2j). The electrostatic waves are typically attributed to lower hybrid drift (LHD) instability driven by the density gradient at the front (e.g., Divin, Khotyaintsev, Vaivads, & André, 2015; Khotyaintsev et al., 2011; Zhou et al., 2009). These LHD waves can heat electrons in the parallel direction (e.g., Divin, Khotyaintsev, Vaivads, André, Markidis, et al., 2015) and may account for the increase of electron parallel temperature behind the jet (Figure 2e).

We further analyze the jet properties in a local DF coordinate system LMN. To establish this system, we perform the minimum variance analysis (MVA) on **B**, which yields L = [0.20, 0.11, 0.97], M = [0.63, −0.78, −0.04], and N = [0.75, 0.63, −0.22]. The ratio between the intermediate eigenvalue and the minimum eigenvalue is about 102, indicating that the MVA analysis is reliable. Also, the ratio between the maximum eigenvalue and the intermediate eigenvalue is about 44, meaning that the DF might be a 1-D structure (Sonnerup & Scheible, 1998). The DF normal direction obtained from the MVA analysis is approximately consistent with that from timing analysis (see also Fu et al., 2012b).

We investigate the ion and electron velocity in the LMN coordinates in Figures 3b–3d. As can be seen, the fast electron jet (V_e ~2,000 km/s) is along the DF tangential direction (Figure 3c), same as the current direction reported in previous studies (e.g., Fu et al., 2012b; Runov et al., 2011). In the normal direction, we see that the electron velocity keeps roughly steady across the DF (Figure 3c). Interestingly, there is an electron flow in the L direction at the DF (~1,000 km/s; see Figure 3d). This electron flow may result in a parallel current at the DF that is theoretically associated with the DF (e.g., Sun et al., 2013). We further investigate the frozen-in condition and the electric-field structure using the generalized Ohm's law (Figures 3e–3g). Clearly, the frozen-in condition for ions is valid inside the ambient plasma and the FPR but is broken at the DF. The Hall effect dominates at the DF, indicating that the frozen-in condition for electrons approximately holds, consistent with previous studies (e.g., Fu et al., 2012b; Yao et al., 2017). The electric field is dominated by E_n (up to 16 mV/m; see Figure 3f), mainly attributed to the Hall effect at the front (e.g., Fu et al., 2012b; Lu et al., 2013). E_l is almost zero during the whole interval (Figure 3g), indicating the absence of parallel electric field. E_m changes smoothly across the DF (Figure 3e) and probably is related to the dawn-dusk electric field in the magnetotail.

Figures 3h–3j display the current structure in LMN coordinates. We compare the four-spacecraft averaged current calculated from the particle moments $J = q_e \cdot n_e \cdot (\boldsymbol{V}_i - \boldsymbol{V}_e)$, with that from curlometer (Figures 3h–3j). We find that the results from the two methods are in good agreement. Since electrons move much faster than ions (see Figures 3b–3d), the current at the DF is primarily carried by the fast electrons. This is consistent with previous suggestions (e.g., Zhang et al., 2011). In fact, the DF current (Figures 3h–3j) has a very similar tendency as the electron velocity (Figures 3b–3d). We notice that the current at the DF is primarily in the tangential plane (J_m is up to 100 nA/m^2; see Figure 3h), consistent with previous observations (e.g., Fu et al.,

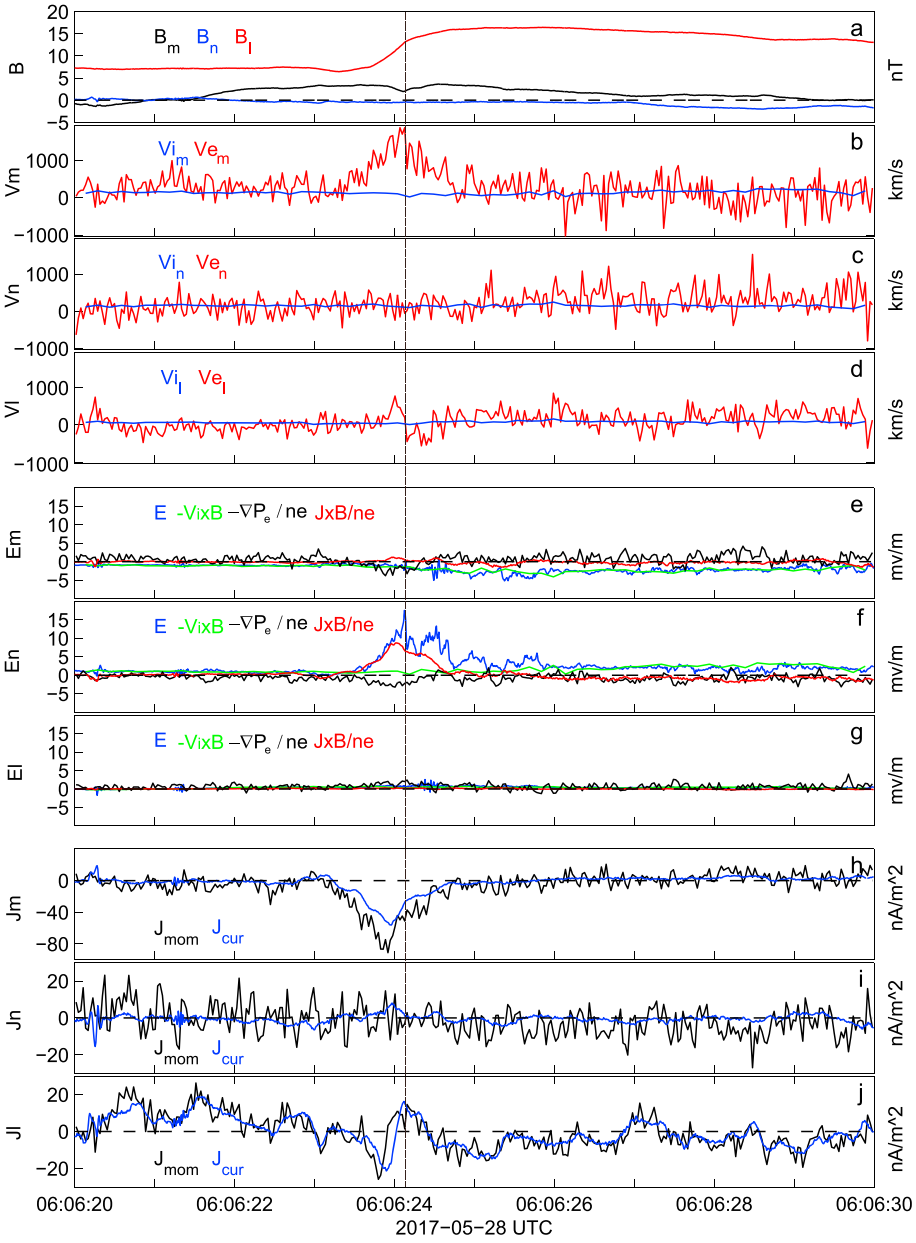

Figure 3. Investigations of electron properties in the LMN coordinates. (a) The B_l, B_m, and B_n components of magnetic field; the (b) *n*, (c) *m*, and (d) *l* components of ion velocity and electron velocity, respectively; the (e) E_l, (f) E_m, and (g) E_n components of electric field; the (h) *n*, (i) *m*, and (j) *l* components of current density from curlometer $\mathbf{J}_{cur}$ (blue) and from particle moments $\mathbf{J}_{mom}$ (black), respectively. The blue (green, black, and red) lines in Figures 3e–3g describe the electric field from EDP (convection term, electron pressure gradient term, Hall term).

2012b). A bipolar signature of J_l—known as localized ring-current—is observed in the jet (Figure 3j). This localized ring-current, primarily in the *L* direction, can cause the decrease of B_m at the front, as observed in Figure 3a.

Due to the strong electric field and current at the front, energy conversion may occur at the DF. We calculate the conversion term, **E**·**J**, by using the current from MMS1 particle moments (Figure 4b) and curlometer (Figure 4c), respectively. Results from the two methods are roughly similar, and their differences stem from the fact that MMS1 cross the DF current sheet a little bit differently than the other three spacecraft. As can be seen, strong energy conversion is observed in the tangential and normal directions at the DF. This

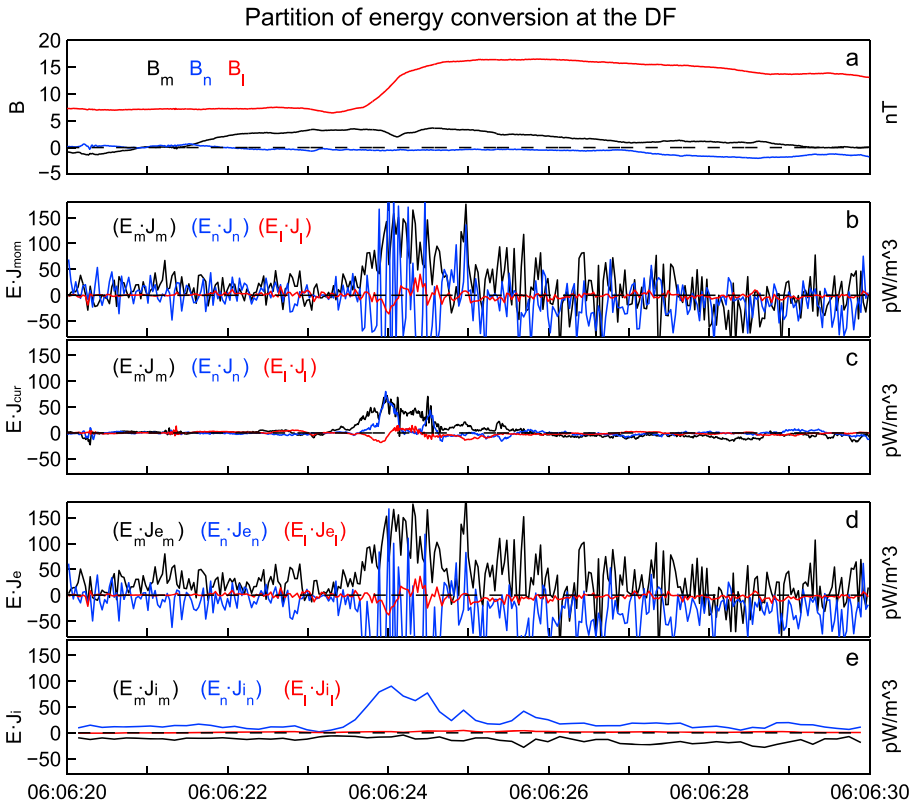

Figure 4. Partition of energy conversion at the DF in LMN coordinates. (a) The B_l, B_m, and B_n components of magnetic field; (b and c) energy conversion resolved using particle moments ($\mathbf{E} \cdot \mathbf{J}_{\mathrm{mom}}$) and Curlometer ($\mathbf{E} \cdot \mathbf{J}_{\mathrm{cur}}$); (d and e) partition of energy conversion to electrons ($\mathbf{E} \cdot \mathbf{J}_e$) and ions ($\mathbf{E} \cdot \mathbf{J}_i$).

conversion is positive ($\mathbf{E} \cdot \mathbf{J} > 0$), indicating the energy transfer from the magnetic field to particles, consistent with previous studies (e.g., Huang, Fu, et al., 2015; Khotyaintsev et al., 2017; Sitnov et al., 2009).

To date, the contribution of ion and electron currents to energy conversion remains an open issue, owing to the lack of electron-velocity measurements. The MMS high-resolution measurements of electron velocity for the first time enable us to investigate this issue. We do this by calculating the energy conversion contributed by ion current ($\mathbf{E} \cdot \mathbf{J}_i$) and electron current $\mathbf{E} \cdot \mathbf{J}_e$ (Figure 4e), respectively. As can be seen, the ion-current-driven energy conversion ($\mathbf{E} \cdot \mathbf{J}_i \approx 80$ pW/m^3) is observed in the normal direction at the front (Figure 4e). Such energy conversion ($\mathbf{E} \cdot \mathbf{J}_i > 0$) is consistent with the picture that the normal electric field can reflect and accelerate the surrounding ions (e.g., Fu et al., 2012b; Zhou et al., 2010). Strong electron-jet-driven energy conversion ($\mathbf{E} \cdot \mathbf{J}_e \approx 150$ pW/m^3) is also observed in the tangential plane (Figure 4d). Note that the electron jet contributes to two-thirds of energy conversion at the DF. Since no increase of electron temperature is observed at the front (Figure 2e), the energy conversion in the tangential plane may thus lead to electron acceleration, that is, consequent increase of the bulk velocity and formation of the jet.

3. Summary

The fast electron jet has been reported at DFs in previous simulations (e.g., Divin, Khotyaintsev, Vaivads, André, Markidis, et al., 2015; Drake et al., 2014; Sitnov et al., 2009) but never been observed by spacecraft. In this study, using MMS measurements, we present the first observation of fast electron jet (V_e ~2,000 km/s) at the DF. Such jet, with scale comparable to the DF thickness (~0.9 d_i), is primarily in the tangential plane. Since electrons are approximately magnetized across the DF, the fast electron jet mainly undergoes the $\mathbf{E} \times \mathbf{B}$ drift motion due to large normal electric fields at the DF.

The electron jet is responsible for the current system at the DF. We find that the role of strong current carried by electron jet in plasma dynamics at the front is significant. For example, it may lead to the current-driven mode instability (the LHD waves) (e.g., Divin, Khotyaintsev, Vaivads, André, Markidis, et al., 2015; Fu et al., 2017), which are indeed observed in this event. The electron-jet-driven current system includes a localized ring-current in the *L* direction, which causes the rotation of the magnetic field line. The electron current contributes to two-thirds of the energy conversion at the DF. This indicates that energy conversion at the DF is dominated by electron current, rather than the ion current suggested in previous studies (e.g., Khotyaintsev et al., 2017; Li et al., 2016; Sitnov et al., 2009).

Acknowledgments
We thank the MMS Science Data Center (https://lasp.colorada.edu/mms/sdc/public/) for providing the data for this study. This work was supported by NSFC grants 41574153, 41431071, and 41404133.

References

Angelopoulos, V., Baumjohann, W., Kennel, C. F., Coroniti, F. V., Kivelson, M. G., Pellat, R., … Paschmann, G. (1992). Bursty bulk flows in the inner central plasma sheet. *Journal of Geophysical Research*, *97*, 4027–4039. https://doi.org/10.1029/91JA02701

Angelopoulos, V., Runov, A., Zhou, X. Z., Turner, D. L., Kiehas, S. A., Li, S. S., & Shinohara, I. (2013). Electromagnetic energy conversion at reconnection fronts. *Science*, *341*(6153), 1478–1482. https://doi.org/10.1126/science.1236992

Ashour-Abdalla, M., El-Alaoui, M., Goldstein, M. L., Zhou, M., Schriver, D., Richard, R., … Hwang, K.-J. (2011). Observations and simulations of non-local acceleration of electrons in magnetotail magnetic reconnection events. *Nature Physics*, *7*, 360–365. https://doi.org/10.1038/nphys1903

Birn, J., Hesse, M., Nakamura, R., & Zaharia, S. (2013). Particle acceleration in dipolarization events. *Journal of Geophysical Research: Space Physics*, *118*, 1960–1971. https://doi.org/10.1002/jgra.50132

Breuillard, H., le Contel, O., Retino, A., Chasapis, A., Chust, T., Mirioni, L., … Nakamura, R. (2016). Multispacecraft analysis of dipolarization fronts and associated whistler wave emissions using MMS data. *Geophysical Research Letters*, *43*, 7279–7286. https://doi.org/10.1002/2016GL069188

Burch, J. L., Moore, T. E., Torbert, R. B., & Giles, B. L. (2015). Magnetospheric multiscale overview and science objectives. *Space Science Reviews*, *199*(1-4), 5–21. https://doi.org/10.1007/s11214-015-0164-9

Cao, J. B., Duan, J., Du, A., Ma, Y., Liu, Z., … Li, Q. (2008). Characteristics of mid-low latitude Pi2 excited by Bursty Bulk Flows. *Journal of Geophysical Research*, *113*, A07S15. https://doi.org/10.1029/2007JA012629

Cao, J. B., Ma, Y. D., Parks, G., Reme, H., Dandouras, I., Nakamura, R., … Zhou, G. C. (2006). Joint observations by Cluster satellites of bursty bulk flows in the magnetotail. *Journal of Geophysical Research*, *111*, A04206. https://doi.org/10.1029/2005JA011322

Divin, A., Khotyaintsev, Y. V., Vaivads, A., & André, M. (2015). Lower hybrid drift instability at a dipolarization front. *Journal of Geophysical Research: Space Physics*, *120*, 1124–1132. https://doi.org/10.1002/2014JA020528

Divin, A., Khotyaintsev, Y. V., Vaivads, A., André, M., Markidis, S., & Lapenta, G. (2015). Evolution of the lower hybrid drift instability at reconnection jet front. *Journal of Geophysical Research: Space Physics*, *120*, 2675–2690. https://doi.org/10.1002/2014JA020503

Drake, J. F., Swisdak, M., Cassak, P. A., & Phan, T. D. (2014). On the 3-D structure and dissipation of reconnection-driven flow bursts. *Geophysical Research Letters*, *41*, 3710–3716. https://doi.org/10.1002/2014GL060249

Duan, A. Y., Cao, J. B., Dunlop, M., & Wang, Z. Q. (2014). Energetic electron bursts in the plasma sheet and their relation with BBFs. *Journal of Geophysical Research: Space Physics*, *119*, 8902–8915. https://doi.org/10.1002/2014JA020169

Ergun, R. E., Tucker, S., Westfall, J., Goodrich, K. A., Malaspina, D. M., Summers, D., … Cully, C. M. (2014). The axial double probe and fields signal processing for the MMS mission. *Space Science Reviews*, *199*(1-4), 167–188. https://doi.org/10.1007/s11214-014-0115-x

Fu, H. S., Cao, J. B., Cully, C. M., Khotyaintsev, Y. V., Vaivads, A., Angelopoulos, V., … Zhima, Z. (2014). Whistler-mode waves inside flux pileup region: Structured or unstructured? *Journal of Geophysical Research: Space Physics*, *119*, 9089–9100. https://doi.org/10.1002/2014JA020204

Fu, H. S., Cao, J. B., Khotyaintsev, Y. V., Sitnov, M. I., Runov, A., Fu, S. Y., … Huang, S. Y. (2013). Dipolarization fronts as a consequence of transient reconnection: In situ evidence. *Geophysical Research Letters*, *40*, 6023–6027. https://doi.org/10.1002/2013GL058620

Fu, H. S., Khotyaintsev, Y. V., André, M., & Vaivads, A. (2011). Fermi and betatron acceleration of suprathermal electrons behind dipolarization fronts. *Geophysical Research Letters*, *38*, L16104. https://doi.org/10.1029/2011GL048528

Fu, H. S., Khotyaintsev, Y. V., Vaivads, A., André, M., & Huang, S. Y. (2012a). Occurrence rate of earthward-propagating dipolarization fronts. *Geophysical Research Letters*, *39*, L10101. https://doi.org/10.1029/2012GL051784

Fu, H. S., Khotyaintsev, Y. V., Vaivads, A., André, M., & Huang, S. Y. (2012b). Electric structure of dipolarization front at sub-proton scale. *Geophysical Research Letters*, *39*, L06105. https://doi.org/10.1029/2012GL051274

Fu, H. S., Khotyaintsev, Y. V., Vaivads, A., André, M., Sergeev, V. A., Huang, S. Y., … Daly, P. W. (2012). Pitch angle distribution of suprathermal electrons behind dipolarization fronts: A statistical overview. *Journal of Geophysical Research*, *117*, A12221. https://doi.org/10.1029/2012JA018141

Fu, H. S., Khotyaintsev, Y. V., Vaivads, A., Retinò, A., & André, M. (2013). Energetic electron acceleration by unsteady magnetic reconnection. *Nature Physics*, *9*(7), 426–430. https://doi.org/10.1038/NPHYS2664

Fu, H. S., Vaivads, A., Khotyaintsev, Y. V., André, M., Cao, J. B., Olshevsky, V., … Retinò, A. (2017). Intermittent energy dissipation by turbulent reconnection. *Geophysical Research Letters*, *44*, 37–43. https://doi.org/10.1002/2016GL071787

Gabrielse, C., Angelopoulos, V., Runov, A., & Turner, D. L. (2012). The effects of transient, localized electric fields on equatorial electron acceleration and transport toward the inner magnetosphere. *Journal of Geophysical Research*, *117*, A10213. https://doi.org/10.1029/2012JA017873

Huang, S. Y., Fu, H. S., Yuan, Z. G., Zhou, M., Fu, S., Deng, X. H., … Yu, X. D. (2015). Electromagnetic energy conversion at dipolarization fronts: Multispacecraft results. *Journal of Geophysical Research: Space Physics*, *120*, 4496–4502. https://doi.org/10.1002/2015JA021083

Huang, S. Y., Yuan, Z. G., Ni, B., Zhou, M., Fu, H. S., Fu, S., … Yu, X. D. (2015). Observations of large-amplitude electromagnetic waves and associated wave-particle interactions at the dipolarization front in the Earth's magnetotail: A case study. *Journal of Atmospheric and Solar: Terrestrial Physics*, *129*, 119–127. https://doi.org/10.1016/j.jastp.2015.05.007

Huang, S. Y., Zhou, M., Deng, X. H., Yuan, Z. G., Pang, Y., Wei, Q., … Wang, Q. Q. (2012). Kinetic structure and wave properties associated with sharp dipolarization front observed by Cluster. *Annales Geophysicae*, *30*, 97–107. https://doi.org/10.5194/angeo-30-97-2012

Hwang, K.-J., Goldstein, M. L., Lee, E., & Pickett, J. S. (2011). Cluster observations of multiple dipolarization fronts. *Journal of Geophysical Research*, *116*, A00I32. https://doi.org/10.1029/2010JA015742

Hwang, K.-J., Goldstein, M. L., Vinas, A. F., Schriver, D., & Ashour-Abdalla, M. (2014). Wave-particle interactions during a dipolarization front event. *Journal of Geophysical Research: Space Physics*, *119*, 2484–2493. https://doi.org/10.1002/2013JA019259

Khotyaintsev, Y. V., Cully, C. M., Vaivads, A., André, M., & Owen, C. J. (2011). Plasma jet braking: Energy dissipation and nondiabatic electrons. *Physical Review Letters*, *106*, 165001. https://doi.org/10.1103/PhysRevLett.106.165001

Khotyaintsev, Y. V., Divin, A., Vaivads, A., André, M., & Markidis, S. (2017). Energy conversion at dipolarization fronts. *Geophysical Research Letters*, *44*, 1234–1242. https://doi.org/10.1002/2016GL071909

Le Contel, O., Leroy, P., Roux, A., Coillot, C., Alison, D., Bouabdellah, A., … de la Porte, B. (2014). The search-coil magnetometer for MMS. *Space Science Reviews*, *199*(1-4), 257–282. https://doi.org/10.1007/s11214-014-0096-9

Li, J.-Z., Zhou, X.-Z., Angelopoulos, V., Liu, J., Runov, A., Pan, D.-X., & Zong, Q.-G. (2016). Contribution of ion reflection to the energy budgets of dipolarization fronts. *Geophysical Research Letters*, *43*, 493–500. https://doi.org/10.1002/2015GL067300

Lindqvist, P.-A., Olsson, G., Torbert, R. B., King, B., Granoff, M., Rau, D., … Tucker, S. (2014). The spin-plane double probe electric field instrument for MMS. *Space Science Reviews*, *199*(1-4), 137–165. https://doi.org/10.1007/s11214-014-0116-9

Liu, C. M., Fu, H. S., Cao, J. B., Xu, Y., Yu, Y. Q., Kronberg, E. A., & Daly, P. W. (2017). Rapid pitch angle evolution of suprathermal electrons behind dipolarization fronts. *Geophysical Research Letters*, *44*, 10,116–10,124. https://doi.org/10.1002/2017GL075007

Liu, C. M., Fu, H. S., Xu, Y., Cao, J. B., & Liu, W. L. (2017). Explaining the rolling-pin distribution of suprathermal electrons behind dipolarization fronts. *Geophysical Research Letters*, *44*, 6492–6499. https://doi.org/10.1002/2017GL074029

Liu, C. M., Fu, H. S., Xu, Y., Wang, T. Y., Cao, J. B., Sun, X. G., & Yao, Z. H. (2017). Suprathermal electron acceleration in the near-Earth flow rebounce region. *Journal of Geophysical Research: Space Physics*, *122*, 594–604. https://doi.org/10.1002/2016JA023437

Liu, J., Angelopoulos, V., Runov, A., & Zhou, X.-Z. (2013). On the current sheets surrounding dipolarizing flux bundles in the magnetotail: The case for wedgelets. *Journal of Geophysical Research: Space Physics*, *118*, 2000–2020. https://doi.org/10.1002/jgra.50092

Lu, H. Y., Cao, J. B., Zhou, M., Fu, H. S., Nakamura, R., Zhang, T. L., … Tao, D. (2013). Electric structure of dipolarization fronts associated with interchange instability in the magnetotail. *Journal of Geophysical Research: Space Physics*, *118*, 6019–6025. https://doi.org/10.1002/jgra.50571

Lu, S., Angelopoulos, V., & Fu, H. S. (2016). Suprathermal particle energization in dipolarization fronts: Particle-in-cell simulations. *Journal of Geophysical Research: Space Physics*, *121*, 9483–9500. https://doi.org/10.1002/2016JA022815

Ma, Y. D., Cao, J. B., Nakamura, R., Zhang, T. L., Reme, H., Dandouras, I., … Dunlop, M. (2009). Statistical analysis of earthward flow bursts in the inner plasma sheet during substorms. *Journal of Geophysical Research: Space Physics*, *114*, A07215. https://doi.org/10.1029/2009JA014275

Nakamura, R., Baumjohann, W., Klecker, B., Bogdanova, Y., Balogh, A., Rème, H., … Runov, A. (2002). Motion of the dipolarization front during a flow burst event observed by Cluster. *Geophysical Research Letters*, *29*(20), 1942. https://doi.org/10.1029/2002GL015763

Pan, Q., Ashour-Abdalla, M., El-Alaoui, M., Walker, R. J., & Goldstein, M. L. (2012). Adiabatic acceleration of suprathermal electrons associated with dipolarization fronts. *Journal of Geophysical Research*, *117*, A12224. https://doi.org/10.1029/2012JA018156

Panov, E. V., Artemyev, A. V., Baumjohann, W., Nakamura, R., & Angelopoulos, V. (2013). Transient electron precipitation during oscillatory BBF braking: THEMIS observations and theoretical estimates. *Journal of Geophysical Research: Space Physics*, *118*, 3065–3076. https://doi.org/10.1002/jgra.50203

Pollock, C., Moore, T., Jacques, A., Burch, J., Gliese, U., Saito, Y., … Zeuch, M. (2016). Fast plasma investigation for magnetospheric multiscale. *Space Science Reviews*, *199*(1-4), 331–406. https://doi.org/10.1007/s11214-016-0245-4

Runov, A., Angelopoulos, V., Sitnov, M. I., Sergeev, V. A., Bonnell, J., McFadden, J. P., … Auster, U. (2009). THEMIS observations of an earthward-propagating dipolarization front. *Geophysical Research Letters*, *36*, L14106. https://doi.org/10.1029/2009GL038980

Runov, A., Angelopoulos, V., Zhou, X.-Z., Zhang, X.-J., Li, S., Plaschke, F., & Bonnell, J. (2011). A THEMIS multicase study of dipolarization fronts in the magnetotail plasma sheet. *Journal of Geophysical Research*, *116*, A05216. https://doi.org/10.1029/2010JA016316

Russell, C. T., Anderson, B. J., Baumjohann, W., Bromund, K. R., Dearborn, D., Fischer, D., … Richter, I. (2014). The magnetospheric multiscale magnetometers. *Space Science Reviews*, *199*(1-4), 189–256. https://doi.org/10.1007/s11214-014-0057-3

Schmid, D., Nakamura, R., Volwerk, M., Plaschke, F., Narita, Y., Baumjohann, W., … Kepko, E. L. (2016). A comparative study of dipolarization fronts at MMS and Cluster. *Geophysical Research Letters*, *43*, 6012–6019. https://doi.org/10.1002/2016GL069520

Sergeev, V., Angelopoulos, V., Apatenkov, S., Bonnell, J., Ergun, R., Nakamura, R., … Runov, A. (2009). Kinetic structure of the sharp injection/dipolarization front in the flow-braking region. *Geophysical Research Letters*, *36*, L21105. https://doi.org/10.1029/2009GL040658

Sitnov, M. I., Swisdak, M., & Divin, A. V. (2009). Dipolarization fronts as a signature of transient reconnection in the magnetotail. *Journal of Geophysical Research*, *114*, A04202. https://doi.org/10.1029/2008JA013980

Sonnerup, B. U., & Scheible, M. (1998). Minimum and maximum variance analysis. In G. Paschmann, & P. W. Daly (Eds.), *Analysis methods for multi-spacecraft data*, (pp. 185–220, ISSI SR-001). Noordwijk, Netherlands: ESA Publ. Div.

Sun, W. J., Fu, S. Y., Parks, G. K., Liu, J., Yao, Z. H., Shi, Q. Q., … Xiao, T. (2013). Field-aligned currents associated with dipolarization fronts. *Geophysical Research Letters*, *40*, 4503–4508. https://doi.org/10.1002/grl.50902

Wu, M. Y., Lu, Q. M., Volwerk, M., Vörös, Z., Zhang, T. L., Shan, L. C., & Huang, C. (2013). A statistical study of electron acceleration behind the dipolarization fronts in the magnetotail. *Journal of Geophysical Research: Space Physics*, *118*, 4804–4810. https://doi.org/10.1002/jgra.50456

Yang, J., Cao, J. B., Fu, H. S., Wang, T. Y., Liu, W. L., & Yao, Z. H. (2017). Broadband high-frequency waves detected at dipolarization fronts. *Journal of Geophysical Research: Space Physics*, *122*, 4299–4307. https://doi.org/10.1002/2016JA023465

Yao, Z., Rae, I. J., Guo, R. L., Fazakerley, A. N., Owen, C. J., Nakamura, R., … Zhang, X.-J. (2017). A direct examination of the dynamics of dipolarization fronts using MMS. *Journal of Geophysical Research: Space Physics*, *122*, 4335–4347. https://doi.org/10.1002/2016JA023401

Yao, Z. H., Liu, J., Owen, C. J., Forsyth, C., Rae, I. J., Pu, Z. Y., … Chu, X. N. (2015). A physical explanation for the magnetic decrease ahead of dipolarization fronts. *Annales de Geophysique*, *33*(10), 1301–1309. https://doi.org/10.5194/angeo-33-1301-2015

Zhang, X.-J., Angelopoulos, V., Runov, A., Zhou, X.-Z., Bonnell, J., McFadden, J. P., … Auster, U. (2011). Current carriers near dipolarization fronts in the magnetotail: A THEMIS event study. *Journal of Geophysical Research*, *116*, A00I20. https://doi.org/10.1029/2010JA015885

Zhou, M., Ashour-Abdalla, M., Deng, X., Schriver, D., El-Alaoui, M., & Pang, Y. (2009). THEMIS observation of multiple dipolarization fronts and associated wave characteristics in the near-Earth magnetotail. *Geophysical Research Letters*, *36*, L20107. https://doi.org/10.1029/2009GL040663

Zhou, M., Ni, B., Huang, S., Deng, X., Ashour-Abdalla, M., Nishimura, Y., … Li, H. (2014). Observation of large-amplitude magnetosonic waves at dipolarization fronts. *Journal of Geophysical Research: Space Physics*, *119*, 4335–4347. https://doi.org/10.1002/2014JA019796

Zhou, X. Z., Angelopoulos, V., Sergeev, V. A., & Runov, A. (2010). Accelerated ions ahead of earthward propagating dipolarization fronts. *Journal of Geophysical Research*, *115*, A00I03. https://doi.org/10.1029/2010JA015481